Advanced Flight Dynamic Modelling of Variable Pitch Quadrotor

Vishnu S. Chipade* , Abhishek† , Mangal Kothari†

Department of Aerospace Engineering,

Indian Institute of Technology Kanpur, Kanpur, UP, India - 208016

The need for high endurance quadrotor has created interest in design and development of variable pitch quadrotors powered by fuel engines. The use of fuel engine enables great scalability, high payload capacity and dramatically high endurance, making it ideal replacement of conventional battery powered quadrotor UAVs for many tasks such search and rescue operations, surveillance, package delivery etc. The control design for a variable pitch quadrotor poses new challenges and it has not been investigated completely. The control design requires flight dynamics model for the variable pitch quadrotor. Mostly, researchers have been using simplified hover based flight dynamic model for control law development and testing. But, this hover based mathematical model is insufficient to model the dynamic behavior of the quadrotor away from a hover condition. In this paper, an advanced flight dynamic model describing generalized motion of the variable pitch quadrotor is developed using Blade Element Momentum Theory (BEMT) and Drees' inflow model for non-uniform induced velocity field. The thrust and torque predicted by the aerodynamic model (rotor dynamics) used within the flight dynamic analysis are validated through experimental results. Similarly, the dynamic response of the variable pitch quadrotor for a given set of control inputs is validated through flight experiments by implementing a PID based control on variable pitch quadrotor.

Nomenclature

A	Rotor disk area
c	Chord
$C_d,\ C_{d_0}$	Coefficient of drag, constant 2D coefficient of drag
C_{Fd}, C_{Fs}, C_{Ft}	Coefficient of drag force, side-force and thrust respectively
C_l, C_{l_α}	Coefficient of lift and lift curve slope for airfoil respectively
C_{Md}, C_{Ms}, C_{Mt}	Coefficients of moments about d, s and t axis respectively
C_Q	Coefficient of torque
C_T	Coefficient of thrust
$(d,\ s,\ t)$	Rotor fixed non-rotating coordinate frame
dL, dD	Elemental lift and drag respectively
$\mathbf{F}$	Vector representing total forces on quadrotor
$\mathbf{F}_{aero}$	Vector representing aerodynamic forces on quadrotor
$\mathbf{F}_{gravity}$	Vector representing gravity force on quadrotor
$F_d,\ F_s$	Rotor drag force along drag and side force axis respectively
dF_x, dF_z	Elemental forces in local rotating x_r and z_r axes respectively
$F_x,\ F_y,\ F_z$	Total external forces in $x_b,\ y_b,\ z_b$ directions
$\mathbf{H}$	Vector representing total angular momentum of quadrotor
g	Acceleration due to gravity, $g = 9.8m/s^2$
I_{xx}, I_{yy}, I_{zz}	Moments of inertia about $x_b,\ y_b,\ z_b$ axes respectively
$k_x,\ k_y$	Weighting factors for deviation of inflow from uniform inflow

*Graduate Student, Department of Aerospace Engineering, Indian Institute of Technology Kanpur, India.

†Assistant Professor, Department of Aerospace Engineering, Indian Institute of Technology Kanpur, India, Member AIAA.

K_F, K_M	Rotor force and moment constant respectively
l_a	Rotor moment arm
l, m, n	Total moments about $x_b,\ y_b,\ z_b$ axes respectively
M	Mass of a variable pitch quadrotor
N_b	Number of blades
$(p,\ q,\ r)$	Body angular rates
$\mathbf{P}$	Vector representing total momentum of quadrotor
q_0	Dynamic pressure
$\mathbf{r_e}$	Position vector with respect to earth fixed frame
R	Rotor blade radius
R_b^e	Transformation matrix from body to earth fixed frame
Re	Reynolds number
T	Total thrust
$(u,\ v,\ w)$	Translational velocities in body fixed frame
U_r, U_R	Sectional resultant and in-plane radial velocity respectively
U_T, U_P	Sectional in-plane tangential and out of plane velocity respectively
$\mathbf{V}_b,\ \mathbf{V}_e$	Velocity vector in body frame and earth frame respectively
$V_c,\ v_i$	Climb and induced velocity respectively
V_{c_j}	Climb velocity for j^{th} rotor
$V_x,\ V_y,\ V_z$	Air velocities in $x_b,\ y_b,\ z_b$ axes respectively
$V_{x_j},\ V_{y_j},\ V_{z_j}$	Air velocities in $x_b,\ y_b,\ z_b$ axes respectively for j^{th} rotor
$(x,\ y,\ z)$	Position coordinates of quadrotor
$(x_e,\ y_e,\ z_e)$	Earth fixed coordinate frame
$(x_b,\ y_b,\ z_b)$	Body fixed coordinate frame
$(x_r,\ y_r,\ z_r)$	Rotor fixed rotating coordinate frame
α	Angle of attack
β	Angle between rotor in-plane flow velocity and x_b axis
β_j	Angle between rotor in-plane flow velocity and x_b axis for j^{th} rotor
$\boldsymbol{\eta}$	Euler angles vector
θ_0	Blade pitch angle
λ_c	Non-dimensional climb velocity
λ_i, λ_{i0}	Non-dimensional induced and mean induced velocity respectively
μ, μ_C	Advance ratio, its component in chord-wise direction respectively
ξ	Non-dimensional radial position, $= y_r/\mathrm{R}$
ρ	Air density
$\rho_y,\ \rho_d,\ \rho_s$	Location of blade element along radius, d and s axis respectively
σ	solidity $=\frac{N_b c}{\pi R}$
$\boldsymbol{\tau}$	Vector representing total moments acting on quadrotor
$(\phi,\ \theta,\ \psi)$	Euler angles representing attitude of quadrotor
Φ	Inflow angle
χ	Wake skew angle
Ψ	Azimuth angle
$\boldsymbol{\Omega}$	Angular rate vector
Ω_r	Rotational speed of rotors

I. Introduction

Recently explosion in the Unmanned Aerial Vehicles (UAVs) market has increased the interest in UAVs. Small UAVs are now extensively researched due to their myriad applications including, but not limited to, search and rescue operations, surveillance, terrain mapping, package delivery, precision agriculture etc. There are different types of UAVs—fixed wing UAVs such as RQ-4 Global Hawk,[1] rotary wing UAVs,[2,3] hybrid vertical take-off landing (VTOL) UAVs,[4] Tail-sitter UAVs,[5] cycloidal rotor UAV.[6] Among all the UAVs, rotary wing UAVs are widely used for commercial applications because of their hover and VTOL capability. Quadrotors have emerged out to be the most popular design because of ease of construction and

simplified control design.

Conventional quadrotors, shown in Fig. 1 (a), have blades with fixed pitch and are controlled by varying rotor RPM. Though mechanically simple, they have limited control bandwidth as reported by.[7] As the quadrotor size increases, this limited control bandwidth can pose challenges for quadrotor controller design,[8] as the inertia of the motors increase and the torque required to change the speed of the motor exceeds its capacity. Typically, these quadrotors use battery as power source which limits their endurance as well as payload capacity. Quadrotor with variable pitch control, shown in Fig. 1 (b), addresses some of these issues. Addition of variable pitch mechanism makes the design mechanically complicated, but improved control bandwidth and reverse thrust producing capability overshadow the increased complexity in the design. Moreover, rotors in variable pitch quadrotors are operated at same rotational speed which offers the possibility of use of single fuel engine power plant, thereby improving endurance significantly, as gasoline has exceptionally high energy density compared to existing lithium polymer batteries commonly used in small UAVs. One such gasoline engine powered variable pitch quadrotor has been designed and developed at Micro Air Vehicle Lab, IIT Kanpur.[9] The mechanism for generating total forces and moments on the variable pitch quadrotor is similar to that for conventional quadrotor except the fact that, the thrust variation of individual rotor is obtained through blade pitch change rather than changing the RPM.

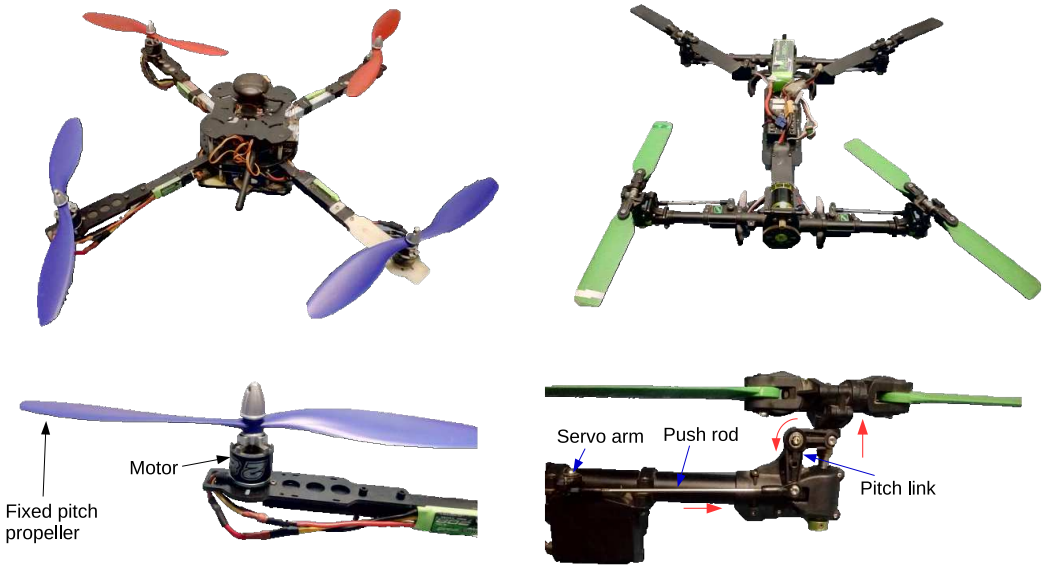

(a) Conventional quadrotor (Built at MAV lab, IIT Kanpur)

(b) Variable pitch quadrotor (Assault Reaper 500)

Figure 1: Conventional and variable pitch quadrotor

A. Literature Survey

Variable pitch propeller based quadrotors is not a contemporary idea. It has been researched in the past as well but researchers were unable to keep the interest alive for variable pitch quadrotors, perhaps, because of the paucity of technological development during those times. Georges de Bothezat and Ivan Jerome, in 1922, built and flew a quadrotor, with variable pitch mechanism for control, named 'Flying Octopus'.[10] Another attempt at full scale variable pitch quadrotor was made by designer D. H. Kaplan in 1956 with Convertawings Model A.[11] The vehicle was powered by two engines driving four rotors through a system of v-belts. It was flown successfully many times in the mid-1950s.

In recent past, some researchers have tried to study the flight mechanics and control of the variable pitch quadrotor in a systematic way.[7,12,13] Cutler *et al.*[7] compared fixed and variable pitch quadrotor and found that variable pitch control mechanism provides faster rate of thrust change, decreased control saturation, and is able to reverse the thrust thereby proliferating the possibilities for aerobatics and other belligerent maneuvers. Tao[14] has designed and fabricated an engine powered variable pitch quadrotor prototype. Tao also designed flight controller using simplified rotor dynamics model based on experiments and BEMT based

rotor dynamics in hover. Flight experiments were conducted to demonstrate the performance and reliability of the mechanical design and controller.

Plenty of literature is available which studied dynamics, stability and control of conventional quadrotors. Martinez[15] has modeled quadrotor dynamics using blade element theory (BET) and Glauert's linear inflow model that are used to model a conventional helicopter rotor dynamics. The momentum theory, used for mean induced velocity, is modified to handle the critical flow conditions during vertical descent. This model considers flapping of the rotors and assumes the rotor to be rectangular. The author developed a MATLAB simulation to study the open loop response of the model, albeit the results were not corroborated with the experimental data. The forward-flight model considering mutual interference between the four rotors was studied in.[16] A mutual-interference model was established for a four rotor system using a rotor disc apparent vortex system that simplified the complex wake structure induced by the four-rotor system in forward flight. A comprehensive computational fluid dynamics analysis is performed to validate the model which confirmed the mutual interference of wakes reasonably well.

Gupta *et. al* in[17] have developed a hover based flight dynamics model for variable pitch quadrotor using blade element momentum theory (BEMT) and developed NDI control. But, not much of efforts have gone into developing reasonably accurate mathematical models for generalized motion of variable pitch quadrotor.

B. Motivation and Overview

With increased popularity of Internet shopping, E-commerce sector faces a daunting task of delivering the packages on time. The technological development in Unmanned Aerial Vehicle (UAVs) has provided the sector a plausible solution that can not only deliver the packages on time but also to remote areas with difficult terrains. E-commerce websites are showing great enthusiasm in UAVs with small payload capacity, as it can augment their profit by cutting manual labor. Apart from Ecommerce sector, military is also showing interest in UAVs with automatic payload delivery system, which will be very conducive during disaster management. These UAVs can be of great strategic importance to the armed forces or may help save lives by dropping the payload for military base camps or during natural calamities or save lives by delivering medicines to inaccessible areas.

All these require the UAVs to operate autonomously, have long range, high endurance and high lifting capacity. Quadrotors or their variants have seen great popularity in this context, but conventional quadrotors suffer when it comes to high endurance, long range, or high lifting capacity. Variable pitch quadrotor, as discussed above, can provide a better solution. But, very limited research has gone into variable pitch quadrotor.

In order to facilitate variable pitch quadrotor to fly autonomously, robust controllers have to developed. Moreover, it is extremely helpful that these controllers are tested with a simulation model before implementing them on real vehicles and analyze the dynamic behavior of the variable pitch quadrotor. Hence, the accuracy of the model (and thus the level of detail) has to be in accordance with the requirements of this task.

In this paper, an advanced descriptive flight dynamics model for a generalized motion of variable pitch quadrotor is developed using blade element momentum theory (BEMT), wherein Drees' inflow model is used to model the non-uniform induced velocity field. The model does not make small angle assumption that general blade element theory (BET) makes. This model also includes the effect of rotational motion of the quadrotor on the relative air velocities that the individual rotors experience. The thrust and torque predictions from the model developed are validated with experimental results for a hover condition. Additionally, the final paper will contain flight experiment results to substantiate the prediction from the mathematical model for a dynamic behavior of the vehicle. The final paper will also contain a brief discussion of simple PID based control developed for variable pitch quadrotor to perform flight experiments.

The paper is organized as follows. Section II details the advanced flight dynamics model. Experimental results are provided in Section III and Section IV concludes the paper.

II. Advanced Flight Dynamics Model

In this section, a mathematical model, which consists of kinematics, vehicle dynamics, and rotor dynamics (aerodynamics), describing the dynamic behaviour of a variable pitch quadrotor during generalized maneuvers is developed.

Two different reference coordinate systems are used for convenience which are shown in Fig. 2. (x_b, y_b, z_b) is the coordinate system attached to body at the center of gravity of the vehicle and (x_e, y_e, z_e) is the inertial frame (earth frame) attached to the fixed point on the earth, where x_e points toward North, y_e toward East and z_e points downward. Initially both the coordinate frames are aligned.

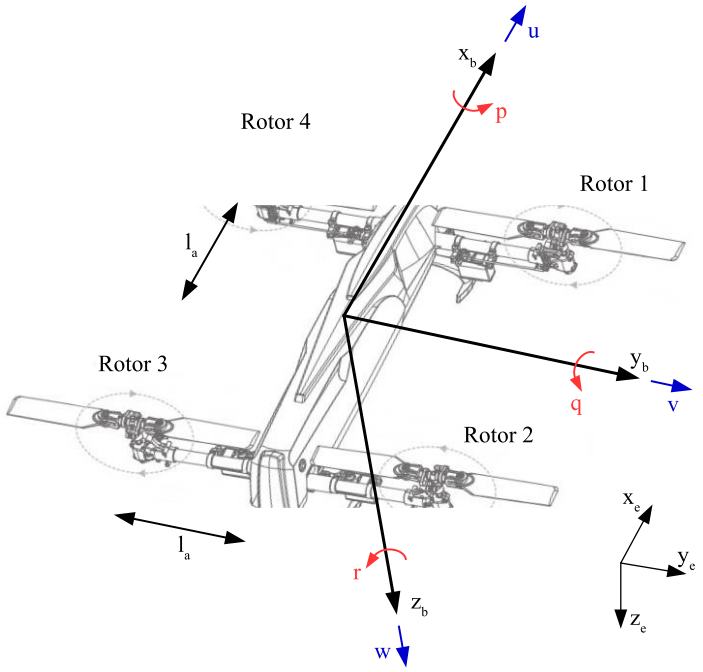

Figure 2: Reference coordinate systems
Source: Instruction Manual for Assault Reaper 500 (https://hobbyking.com/media/file/1014411680X53414X18.pdf)

Following is the rotation matrix which transforms any vector in body frame to an inertial frame.

$$R_b^e = \begin{bmatrix} C\theta C\psi & S\phi S\theta C\psi - C\phi S\psi & C\phi S\theta C\psi + S\phi S\psi \\ C\theta S\psi & S\phi S\theta S\psi + C\phi C\psi & C\phi S\theta S\psi - S\phi C\psi \\ -S\theta & S\phi C\theta & C\phi C\theta \end{bmatrix} \tag{1}$$

where $C\Delta = cos(\Delta)$ and $S\Delta = sin(\Delta)$ for all $\Delta \in \{\phi, \theta, \psi\}$. The transformation from earth to body frame can be obtained as, $R_e^b = (R_b^e)^T$

A. Kinematics

Typically an on-board Inertial Measurement Unit (IMU) is used to measure angular and translational rates in body frame. The translational velocity in earth fixed frame, $\mathbf{V}_e = [\dot{x}\ \dot{y}\ \dot{z}]^T$ and velocity in body frame, $\mathbf{V}_b = [u\ v\ w]^T$ are related as in Eq. (2).

$$\mathbf{V}_e = \dot{\mathbf{r}}_e = \begin{bmatrix} \dot{x} \\ \dot{y} \\ \dot{z} \end{bmatrix} = R_b^e \begin{bmatrix} u \\ v \\ w \end{bmatrix} \tag{2}$$

Similarly, to relate the Euler rates, $\dot{\boldsymbol{\eta}} = [\dot{\phi} \quad \dot{\theta} \quad \dot{\psi}]^T$, that are measured in the inertial frame and angular body rates, $\boldsymbol{\Omega} = [p \quad q \quad r]^T$, a transformation is given in Eq. (3).

$$\dot{\boldsymbol{\eta}} = \begin{bmatrix} \dot{\phi} \\ \dot{\theta} \\ \dot{\psi} \end{bmatrix} = \begin{bmatrix} 1 & \frac{S\phi S\theta}{C\theta} & \frac{C\phi S\theta}{C\theta} \\ 0 & C\phi & -S\phi \\ 0 & \frac{S\phi}{C\theta} & \frac{C\phi}{C\theta} \end{bmatrix} \begin{bmatrix} p \\ q \\ r \end{bmatrix} \tag{3}$$

B. Dynamics

The 6 DOF equations of motion of a variable pitch quadrotor can be derived by applying Newton's laws. It is assumed that the frame of the VP quadrotor is rigid and the individual rotors are also rigid.
Translational dynamics of the quadrotor in inertial frame is given below.

$$\mathbf{F} = M\left[\frac{\mathrm{d}\mathbf{V}_b}{\mathrm{d}t} + \boldsymbol{\Omega} \times \mathbf{V}_b\right]$$

$$\mathbf{F} = \begin{bmatrix} F_x \\ F_y \\ F_z \end{bmatrix} = M\left\{\begin{bmatrix} \dot{u} \\ \dot{v} \\ \dot{w} \end{bmatrix} + \begin{bmatrix} qw - rv \\ ru - pw \\ pv - qu \end{bmatrix}\right\} \tag{4}$$

Here $\mathbf{F} = \mathbf{F}_{aero} + R_e^b \mathbf{F}_{gravity}$. $\mathbf{F}_{aero}$ is a vector representing the aerodynamic forces acting on all the rotors together and quadrotor frame in body frame and $\mathbf{F}_{gravity}$ is gravity force vector defined in earth frame. The aerodynamic forces on the frame are neglected from the formulation as these are negligibly small.

The translational dynamics can also be expressed in inertal earth fixed frame as follows

$$\dot{\mathbf{V}}_e = \frac{1}{M}\left[R_b^e \mathbf{F}_{aero} + \mathbf{F}_{gravity}\right]$$

$$\begin{bmatrix} \ddot{x} \\ \ddot{y} \\ \ddot{z} \end{bmatrix} = \frac{1}{M} R_b^e \begin{bmatrix} F_x^a \\ F_y^a \\ F_z^a \end{bmatrix} + \begin{bmatrix} 0 \\ 0 \\ g \end{bmatrix} \tag{5}$$

Here F_x^a, F_y^a, F_z^a are the aerodynamic forces acting on quadrotor in body fixed x, y, z directions. M is the mass of quadrotor.
Similarly, the rotational Dynamics of the quadrotor is given as below.

$$\boldsymbol{\tau} = \frac{\partial}{\partial t}(I\boldsymbol{\Omega}) + \boldsymbol{\Omega} \times (I\boldsymbol{\Omega})$$

Here $\boldsymbol{\tau}$ is a vector representing summation of total aerodynamic moments acting on all the rotors, the moments on the body because of the aerodynamic forces on the rotors, and aerodynamic moments acting on quadrotor frame. The moments on the frame, similar to forces, are neglected from the formulation as these are negligibly small. There are no gyroscopic moments acting on the vehicle because the speed of all the rotors is same and two of the rotors rotate in one direction while other two rotate in opposite direction, which balance the gyroscopic moments.

$$\dot{\boldsymbol{\Omega}} = I^{-1}\left[-\boldsymbol{\Omega} \times (I\boldsymbol{\Omega}) + \boldsymbol{\tau}\right]$$

$$\begin{bmatrix} \dot{p} \\ \dot{q} \\ \dot{r} \end{bmatrix} = I^{-1}\left(-\begin{bmatrix} p \\ q \\ r \end{bmatrix} \times \left(I\begin{bmatrix} p \\ q \\ r \end{bmatrix}\right) + \begin{bmatrix} l \\ m \\ n \end{bmatrix}\right) \tag{6}$$

Here l, m, n are the total moments acting on quadrotor in body fixed x, y, z directions. I is the moment of inertia matrix for quadrotor. It is reasonable to assume quadrotor to be symmetric, therefore, $I = diag([I_{xx},\ I_{yy},\ I_{zz}])$. This simplifies Eq. (6) to Eq. (7) as follows.

$$\begin{bmatrix} \dot{p} \\ \dot{q} \\ \dot{r} \end{bmatrix} = \begin{bmatrix} \frac{I_{yy} - I_{zz}}{I_{xx}} qr \\ \frac{I_{zz} - I_{xx}}{I_{yy}} pr \\ \frac{I_{xx} - I_{yy}}{I_{zz}} pq \end{bmatrix} + \begin{bmatrix} \frac{l}{I_{xx}} \\ \frac{m}{I_{yy}} \\ \frac{n}{I_{zz}} \end{bmatrix} \tag{7}$$

C. Rotor Dynamics during Generalized Motion

In this section, a rotor dynamics model for a generalized motion of a variable pitch quadrotor is presented. In a variable pitch quadrotor, the thrust of the each rotor is changed by changing the corresponding blade pitch. In general, during a generalized motion, the rotors also encounter an edgewise air flow which leads to periodic variation in local velocity profiles at different rotor locations. The induced velocity profile is no longer uniform and simple to model. But, with some simplifying assumptions, the aerodynamic forces and moments generated by each rotor can be calculated using blade element momentum theory (BEMT).[10] BEMT combines blade element theory (BET) and momentum theory (MT). BET assumes blade elements operating aerodynamically independent of each other and integrates the forces over all such elements and momentum theory assist the calculations of induced velocity field. Here, Drees' inflow model is used to model the non-uniform inflow during the generalized motion of the VP quadrotor alongside the simple momentum theory. Consider a blade element of a rotor blade that is rotating at angular speed of Ω_r as shown in Fig. 3.

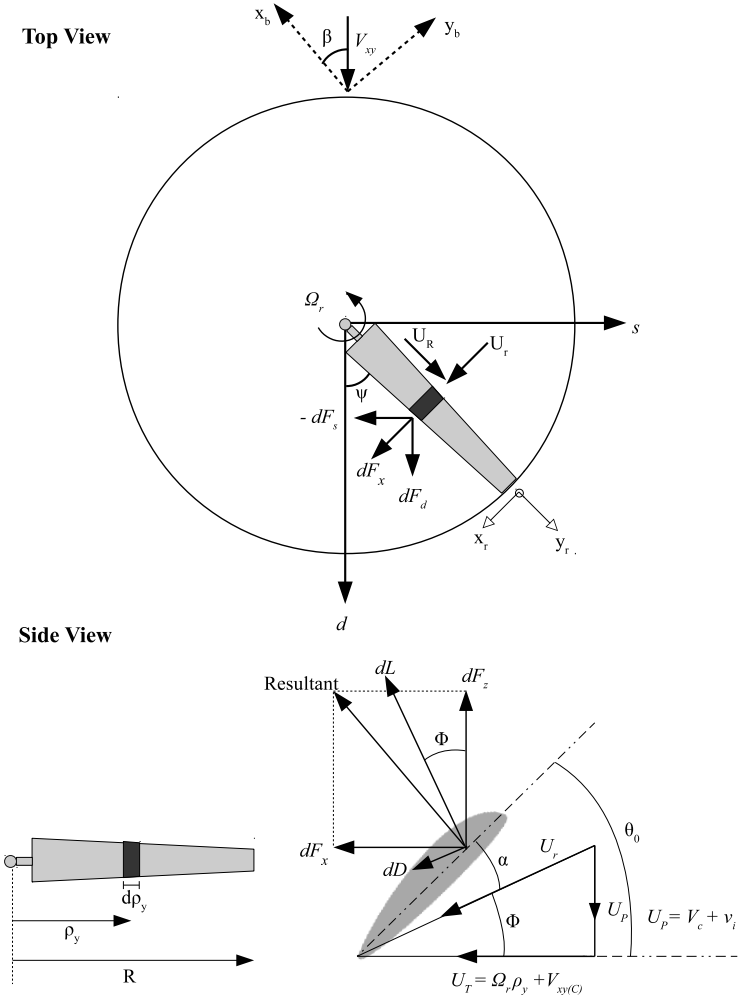

Figure 3: Blade velocity components

According to BET, the elemental forces acting on the blade element are as follows

$$\left.\begin{aligned} dF_z &= dLcos(\Phi) - dDsin(\Phi) \\ dF_x &= dLsin(\Phi) + dDcos(\Phi) \\ dM_z &= -\rho_y dF_x; \\ dM_x &= \rho_y dF_z \end{aligned}\right\} \tag{8}$$

where

$$dL = (\frac{1}{2}\rho U_r^2 c C_l)d\rho_y \qquad dD = (\frac{1}{2}\rho U_r^2 c C_d)d\rho_y$$
$$U_r = \sqrt{U_P^2 + U_T^2} \qquad \left[\text{where} \quad U_P = V_c + v_i; \qquad U_T = \Omega_r \rho_y + V_{xy(C)}\right]$$

Here, $C_l = C_l(\alpha, Re)$ and $C_d = C_d(\alpha, Re)$, where α is angle of attack as defined in Eq. (9) and Re is Reynolds number.

$$\begin{aligned} \alpha &= \theta_0 - \Phi \\ \Phi &= \tan^{-1}\left(\frac{U_P}{U_T}\right) \end{aligned} \tag{9}$$

Since blade radius is small, the Reynolds number variation would be small and hence C_l, C_d can be assumed to be function of α only. The variation of C_l, C_d with α can be obtained using experiments or numerical techniques: computational fluid dynamics (CFD), vortex lattice method (VLM) etc.

In Fig. 3, V_x is the free-stream velocity perpendicular to the rotor disc and v_i is the induced velocity by the rotor. V_{xy} is the free-stream velocity along the rotor disc while $V_{xy(C)} = V_{xy}\sin(\Psi)$ and $V_{xy(R)} = V_{xy}\cos(\Psi)$ are its components along the chord and span of the rotor respectively. The effect due to span-wise component is not considered here. d-axis (drag axis) is along the free-stream in the plane of the rotor disc, s-axis (side-force axis) is perpendicular to it (in the plane) and t-axis (thrust axis) points upward (out of the plane in Fig. 3). From Fig. 3, the elemental forces are resolved along these directions and integrated over the length of the rotor and averaged over a revolution of the rotor.

It is always convenient to work with non-dimensional parameters. Some relevant non-dimensional parameters are defined as follows.

$$\xi \triangleq \frac{\rho_y}{R}; \qquad \sigma(\xi) \triangleq \frac{N_b c(\xi) R}{\pi R^2} \text{ (solidity ratio)}$$
$$\lambda_i \triangleq \frac{v_i}{\Omega_r R}; \quad \lambda_c \triangleq \frac{V_c}{\Omega_r R}; \qquad \mu \triangleq \frac{V_{xy}}{\Omega_r R}; \quad \nu_r \triangleq \frac{U_r}{\Omega_r R}$$
$$\nu_r^2 = (\xi + \mu_C)^2 + (\lambda_c + \lambda_i)^2; \qquad \mu_C \triangleq \frac{V_{xy(C)}}{\Omega_r R} = \mu sin(\Psi)$$

Here, N_b is number of blades, c is chord of the blade.
The elemental forces can be written in non-dimensional form as follows

$$dC_{Ft} = \frac{N_b dF_t}{q_0 A} = \frac{N_b dF_z}{q_0 A} = \frac{1}{2}\sigma(C_l\cos(\Phi) - C_d\sin(\Phi))\nu_r^2 d\xi$$
$$dC_{Fd} = \frac{N_b dF_d}{q_0 A} = \frac{N_b dF_x sin(\Psi)}{q_0 A} = \frac{1}{2}\sigma(C_l\sin(\Phi) + C_d\cos(\Phi))\nu_r^2 sin(\Psi) d\xi$$
$$dC_{Fs} = \frac{N_b dF_s}{q_0 A} = \frac{-N_b dF_x cos(\Psi)}{q_0 A} = -\frac{1}{2}\sigma(C_l\sin(\Phi) + C_d\cos(\Phi))\nu_r^2 cos(\Psi) d\xi$$
$$dC_{Mt} = \frac{N_b dM_t}{q_0 RA} = \frac{N_b dM_z}{q_0 RA} = -\frac{1}{2}\sigma(C_l\sin(\Phi) + C_d\cos(\Phi))\xi\nu_r^2 d\xi$$
$$dC_{Md} = \frac{N_b dM_d}{q_0 RA} = \frac{N_b dM_x sin(\Psi)}{q_0 RA} = \frac{1}{2}\sigma(C_l\cos(\Phi) - C_d\sin(\Phi))\xi\nu_r^2 sin(\Psi) d\xi$$
$$dC_{Ms} = \frac{N_b dM_s}{q_0 RA} = \frac{-N_b dM_x cos(\Psi)}{q_0 RA} = -\frac{1}{2}\sigma(C_l\cos(\Phi) - C_d\sin(\Phi))\xi\nu_r^2 cos(\Psi) d\xi$$

Here, $q_0 = \rho(\Omega_r R)^2$ and $A = \pi R^2$. These elemental forces after integrating over the length of a blade and

averaging over a revolution give the aerodynamic coefficients as in Eq. (10)

$$\left.\begin{aligned}
C_T = C_{Ft} &= \frac{1}{2\pi}\int_0^{2\pi}\int_{\xi_o}^{1} dC_{Ft}d\Psi \\
&= \frac{1}{2\pi}\int_0^{2\pi}\int_{\xi_o}^{1} \frac{1}{2}\sigma(C_l\cos(\Phi) - C_d\sin(\Phi))\nu_r^2 d\xi d\Psi \\
C_{Fd} &= \frac{1}{2\pi}\int_0^{2\pi}\int_{\xi_o}^{1} dC_{Fd}d\Psi \\
&= \frac{1}{2\pi}\int_0^{2\pi}\int_{\xi_o}^{1} \frac{1}{2}\sigma(C_l\sin(\Phi) + C_d\cos(\Phi))\nu_r^2 sin(\Psi) d\xi d\Psi \\
C_{Fs} &= \frac{1}{2\pi}\int_0^{2\pi}\int_{\xi_o}^{1} dC_{Fs}d\Psi \\
&= \frac{1}{2\pi}\int_0^{2\pi}\int_{\xi_o}^{1} -\frac{1}{2}\sigma(C_l\sin(\Phi) + C_d\cos(\Phi))\nu_r^2 cos(\Psi) d\xi d\Psi \\
C_Q = C_{Mt} &= \frac{1}{2\pi}\int_0^{2\pi}\int_{\xi_o}^{1} dC_{Mt}d\Psi \\
&= \frac{1}{2\pi}\int_0^{2\pi}\int_{\xi_o}^{1} -\frac{1}{2}\sigma(C_l\sin(\Phi) + C_d\cos(\Phi))\xi\nu_r^2 d\xi d\Psi \\
C_{Md} &= \frac{1}{2\pi}\int_0^{2\pi}\int_{\xi_o}^{1} dC_{Md}d\Psi \\
&= \frac{1}{2\pi}\int_0^{2\pi}\int_{\xi_o}^{1} \frac{1}{2}\sigma(C_l\cos(\Phi) - C_d\sin(\Phi))\xi\nu_r^2 sin(\Psi) d\xi d\Psi \\
C_{Ms} &= \frac{1}{2\pi}\int_0^{2\pi}\int_{\xi_o}^{1} dC_{Ms}d\Psi \\
&= \frac{1}{2\pi}\int_0^{2\pi}\int_{\xi_o}^{1} -\frac{1}{2}\sigma(C_l\cos(\Phi) - C_d\sin(\Phi))\xi\nu_r^2 cos(\Psi) d\xi d\Psi
\end{aligned}\right\} \quad (10)$$

Induced velocity field

Equation (10) can be integrated to obtain coefficients of various forces acting on the rotor but induced velocity, λ_i, is not known. In generalized motion, this induced velocity field is no longer axisymmetric. This unknown induced velocity depends upon the rotor wake, total thrust, airloads distribution etc. Tip vortices produce a highly non-uniform inflow and determining this would be a daunting task. But, a simpler linear inflow models based on experimental results give reasonable results for force calculations. One of these inflow models, Drees' inflow model,[10] is used here because of its simplicity and reasonably good description of the rotor inflow.

According to Drees' inflow model the inflow variation over the rotor disk is given as below,

$$\lambda_i = \lambda_{i0}(1 + k_x\frac{\rho_d}{R} + k_y\frac{\rho_s}{R}) = \lambda_{i0}(1 + k_x\xi cos(\Psi) + k_y\xi sin(\Psi)) \quad (11)$$

where ρ_d is the location of blade element along the drag axis and ρ_s is the location of the element along the side-force axis. λ_{i0} is the mean induced velocity at the center of the rotor disk as obtained by standard momentum theory in forward flight.[10] k_x, k_y are weighting factors. λ_{i0}, k_x, k_y are defined below.

$$\lambda_{i0} = \frac{C_T}{2\sqrt{\mu^2 + (\lambda_c + \lambda_{i0})^2}} \quad (12)$$

$$\left.\begin{aligned} k_x &= \frac{4}{3}\left(\frac{1-cos(\chi)-1.8\mu^2}{sin(\chi)}\right) \\ k_y &= -2\mu \end{aligned}\right\} \tag{13}$$

where the wake skew angle, shown in Fig. 4, is

$$\chi = \tan^{-1}\left(\frac{\mu}{\lambda_c+\lambda_i}\right) \tag{14}$$

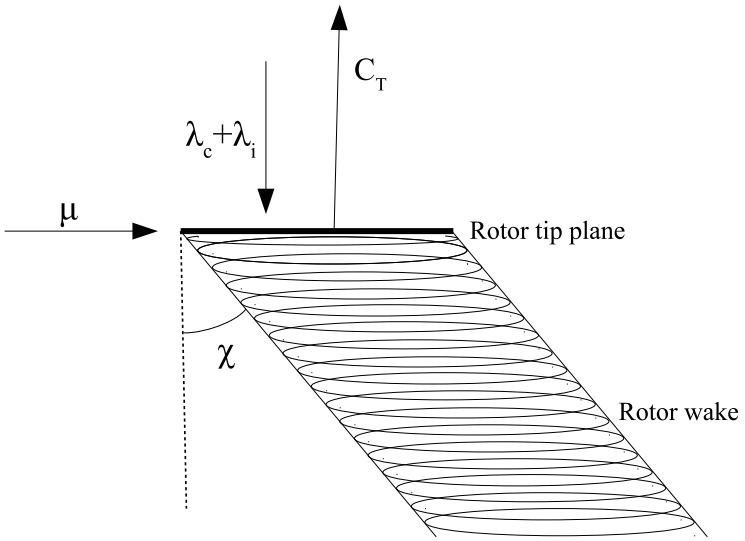

Figure 4: Rotor wake and wake angle

Equation (12) is valid for all flight regimes except during vortex ring state in which the assumption of continuous streamtube, that the simple momentum theory makes, breaks down. When a rotor is descending slowly with low to zero forward speed (a necklace like boundary in $\mu - \lambda$ plane[18]) it enters into vortex ring state in which the flow field is quite complex, there is no defined direction in which the air is flowing. The flow is full of vorticity. During such a flight, the solution from Eq. (11) ceases to be valid. In general, this condition will not arise in typical quadrotor maneuvers and even if this condition occurs for any rotor it will be for very small time and hence the solution from Eq. (12) is used and it is a reasonable assumption.

Since C_T depends on λ_{i0} which in turn depends on C_T, an iterative approach as in[19] is used to obtain the inflow and aerodynamic coefficients. Following is a step by step algorithm that is used to obtain the aerodynamic coefficients.

1. First thrust coefficient C_T is obtained for given pitch input during hover using the expression for C_T as in Eq. (10).

2. This C_T value is given as initial guess, C_{T_0}, to obtain the inflow from Eq. (12) which is solved using Newton Raphson method to obtain λ_{i0}.

3. This is used to obtain aerodynamic coefficients using Eq. (10) at given pitch setting and airflow conditions. The aerodynamic coefficients are obtained by numerically integrating Eq. (10) using Gaussian quadrature rule.

4. These steps are repeated until the relative difference between thrust value C_T^j and initial guess $C_{T_0}^j$ drops below a certain tolerance.

$$\left|\frac{C_T^j - C_{T_0}^j}{C_T^j}\right| \leq \epsilon \tag{15}$$

where $\epsilon = 10^{-5}$ and the initial guess for the next iteration $C_{T_0}^{j+1}$ is updated as $C_{T_0}^{j+1} = C_{T_0}^j + \delta(C_T^j - C_{T_0}^j)$. Where δ is rate of update and its value is 0.1 in this case.

In case of quadrotor, each rotor experiences air velocity components differently during a generalized motion of the vehicle because of the rotational rates. The rotational motion of the quadrotor can significantly affect the forces and moments that each of the rotors produces, hence the effect of rotational motion of the quadrotor is also considered. The velocity components that each of the rotor experiences in any generalized motion are given below.

For Rotor 1:

$$\left.\begin{aligned} V_{x_1} &= u - l_a r \\ V_{y_1} &= v + l_a r \\ V_{c_1} &= -V_{z_1} = -w - l_a p + l_a q \end{aligned}\right\} \quad (16)$$

For Rotor 2:

$$\left.\begin{aligned} V_{x_2} &= u - l_a r \\ V_{y_2} &= v - l_a r \\ V_{c_2} &= -V_{z_2} = -w - l_a p - l_a q \end{aligned}\right\} \quad (17)$$

For Rotor 3:

$$\left.\begin{aligned} V_{x_3} &= u + l_a r \\ V_{y_3} &= v - l_a r \\ V_{c_3} &= -V_{z_3} = -w + l_a p - l_a q \end{aligned}\right\} \quad (18)$$

For Rotor 4:

$$\left.\begin{aligned} V_{x_4} &= u + l_a r \\ V_{y_4} &= v + l_a r \\ V_{c_4} &= -V_{z_4} = -w + l_a p + l_a q \end{aligned}\right\} \quad (19)$$

Here, V_{c_j} is climbing velocity of the j^{th} rotor. Advance ratio for each rotor can be calculated as $\mu_j = \frac{\sqrt{V_{x_j}^2 + V_{y_j}^2}}{V_{tip}}$ and non-dimensionalized climbing speed $\lambda_{c_j} = \frac{V_{c_j}}{\Omega_r R}$ for $\forall j,\ j = \{1, 2, 3, 4\}$. These non-dimensional parameters along with the inflow obtained using Eq. (11) can be used in Eq. (10) to obtain aerodynamic coefficients C_{T_j}, C_{Fd_j}, C_{Fs_j}, C_{Q_j}, C_{Md_j}, C_{Ms_j} for $\forall j,\ j = \{1, 2, 3, 4\}$.

Furthermore, in case of variable pitch quadrotor, two rotors (Rotor 2 and 4, Fig. 2) rotate in anticlockwise direction while other two rotate in clockwise direction. Figure 5 shows comparison of elemental forces on rotor element when the rotor is rotating in clockwise and anticlockwise direction. Consider the coefficients of aerodynamic forces and moments on clockwise rotating rotor are denoted by $\{C_T^{'}, C_{Fd}^{'}, C_{Fs}^{'}, C_Q^{'}, C_{Md}^{'}, C_{Ms}^{'}\}$. It can be observed, from Fig. 5, that these coefficients can be related to the coefficients when the same rotor would be rotating in anticlockwise direction with the same operating conditions, obtained using Eq. (10), as follows.

$$\left.\begin{aligned} C_T^{'} &= C_T; & C_Q^{'} &= -C_Q \\ C_{Fd}^{'} &= C_{Fd}; & C_{Md}^{'} &= -C_{Md} \\ C_{Fs}^{'} &= -C_{Fs}; & C_{Ms}^{'} &= C_{Ms} \end{aligned}\right\} \quad (20)$$

Here, all the coefficients are calculated assuming the rotors are rotating in anticlockwise direction and then their signs are changed according to Eq. (20) to obtain forces for clockwise rotation. These coefficients after multiplying with their respective dimensional coefficients give the forces and moments acting on the respective rotor discs. This gives total forces and moments acting on the quadrotor as follows

$$\left.\begin{aligned} F_x^a &= -K_F \textstyle\sum_{j=1}^{4} (C_{Fd_j} cos(\beta_j) + (-1)^j C_{Fs_j} sin(\beta_j)) \\ F_y^a &= -K_F \textstyle\sum_{j=1}^{4} (C_{Fd_j} sin(\beta_j) - (-1)^j C_{Fs_j} cos(\beta_j)) \\ F_z^a &= -K_F \textstyle\sum_{j=1}^{4} C_{T_j} \end{aligned}\right\} \quad (21)$$

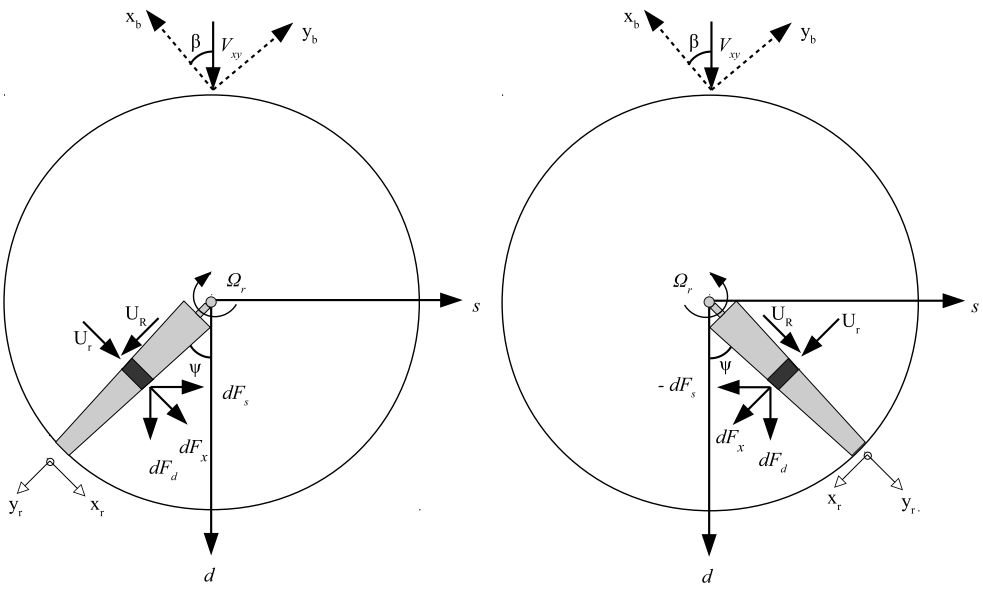

Figure 5: Forces for clockwise rotation of rotor

$$
\left.
\begin{aligned}
l &= l_a K_F \sum_{j=1}^{2}(C_{T_{j+2}} - C_{T_j}) - K_M \sum_{j=1}^{4}\Big[(-1)^j C_{Md_j} cos(\beta_j) + C_{Ms_j} sin(\beta_j)\Big] \\
m &= l_a K_F \sum_{j=1}^{2}(-1)^j(C_{T_{j+2}} - C_{T_j}) - K_M \sum_{j=1}^{4}\Big[(-1)^j C_{Md_j} sin(\beta_j) - C_{Ms_j} cos(\beta_j)\Big] \\
n &= l_a K_F \sum_{j=1}^{2}\Big[C_{Fd_j}\big\{cos(\beta_j) + (-1)^j sin(\beta_j)\big\} - C_{Fd_{j+2}}\big\{cos(\beta_{j+2}) + (-1)^j sin(\beta_{j+2})\big\}\Big] \\
&\quad + \Big[C_{Fs_j}\big\{(-1)^{j+1} cos(\beta_j) + sin(\beta_j)\big\} - C_{Fs_{j+2}}\big\{(-1)^{j+1} cos(\beta_{j+2}) + sin(\beta_{j+2})\big\}\Big] \\
&\quad - K_M \sum_{j=1}^{4}(-1)^j C_{Q_j}
\end{aligned}
\right\} \tag{22}
$$

where $K_F = \rho A(\Omega_r R)^2$, $K_M = K_F R$ and l_a is the moment arm for each rotor.

This model of rotor dynamics along with the equations of kinematics and dynamics gives a more realistic description of quadrotor's motion. These equations can be used to simulate the dynamics of the quadrotor to analyze the variable pitch quarotor's dynamic behavior. This model can also be used to test various control algorithms before they are actually deployed on the hardware systems.

III. Simulation and Experimental Results

The theory developed in Section II is tested in simulations as well as validated by performing set of experiments. The hardware platform chosen for the simulations and flight experiments is a variable pitch quadrotor Assault Reaper 500 sold by HobbyKing. The specifications of the Assault Reaper 500 are listed in Table 1. The inertia values of the quadrotor are estimated approximately. For this, different parts of the quadrotor are approximated as geometric objects with similar shape and for which moments of inertia about their geometric center are well defined in terms of their geometric parameters. Parallel axis theorem is used to finally calculate the moments of inertia about the center of the vehicle.

Table 1: **Quadrotor Parameters**

Mass of quadrotor, M	1.5 Kg
Number of blades, N_b	2
Radius of rotor blades, R	0.14 m
Chord of rotor blades, c	0.028 m
Moment of Inertia, I_{xx}	0.0122 $Kg\ m^2$
Moment of Inertia, I_{yy}	0.0266 $Kg\ m^2$
Moment of Inertia, I_{zz}	0.0387 $Kg\ m^2$

The lift and drag coefficient variation with angle of attack for a symmetric airfoil that is used in rotors of Assault Reaper 500, is shown in Fig. 6. This data is obtained from an online source 'Airfoil tools'.[20]

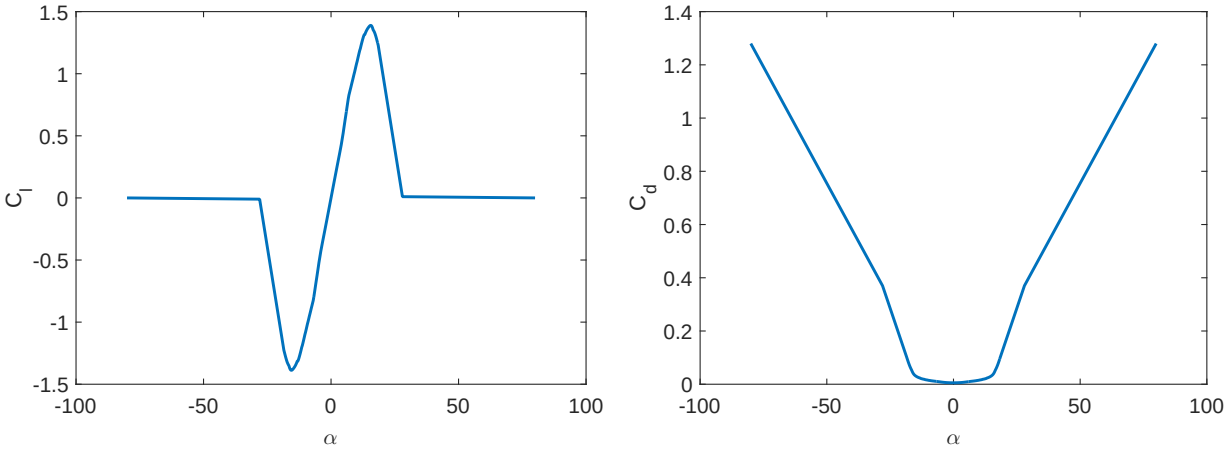

(a) Lift coefficient with angle of attack

(b) Drag coefficient with angle of attack

Figure 6: Aerodynamic coefficients with angle of attack

A. Simulation Results

In this section, simulation results for open loop response of the variable pitch quadrotor are provided. The quadrotor is initially hovering at $(x,\ y,\ z) = (1,\ 1,\ 2)$ which requires the control input, i.e. blade pitch angle, for each rotor to be 13.957^0. After one second, a step input of additional half degree blade pitch angle is applied to the quadrotor. The open loop response of the quadrotor is shown in Figs. 7 and 8. Figure. 7 (a) and (b) show position and velocity of the quadrotor respectively. Similarly, Figure 8 (a) and (b) show Euler angles and their rates respectively As can be observed from Fig. 7 (b), the quadrotors starts rising up, because as we apply an extra blade pitch angle to all the rotors, there is an extra thrust produced in upward direction and the quadrotor starts accelerating in upward direction. z is pointing downwards and hence position and velocity in z direction have negative sign. As can be observed, the velocity in z direction reaches a steady value after some time. It can be attributed to the fact that as the quadrotor starts climbing up the rotors see some relative velocity in perpendicular direction and the thrust produced by each rotor under this operating condition reduces. The point comes when this thrust exactly balances the total weight of the quadrotor and there is no more acceleration in upward direction, hence the velocity becomes steady after time. As can be observed from Fig. 8 the attitude of the quadrotor is not disturbed much when a symmetric input is applied

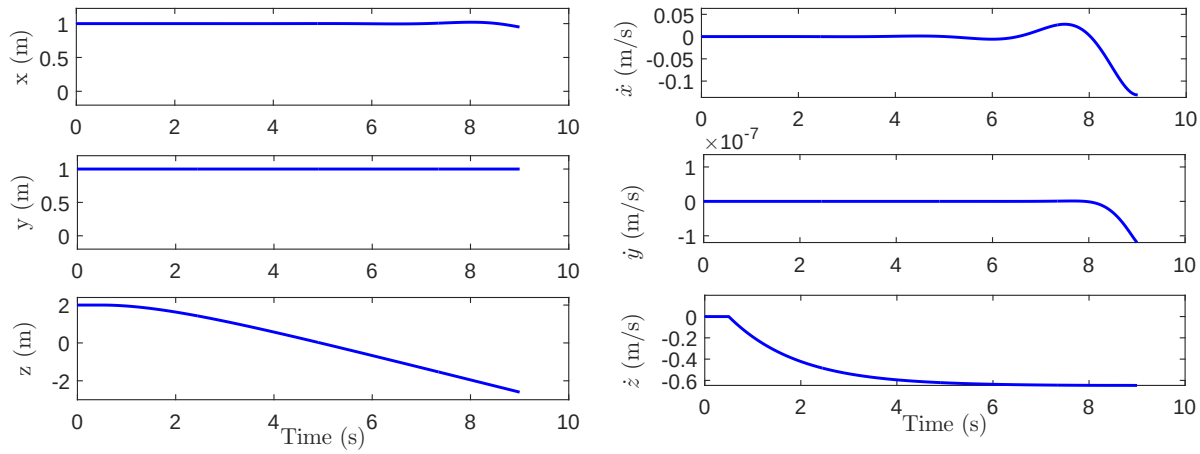

(a) Position with time

(b) Velocity pitch time

Figure 7: Open loop response for symmetric step input to all the rotors (position)

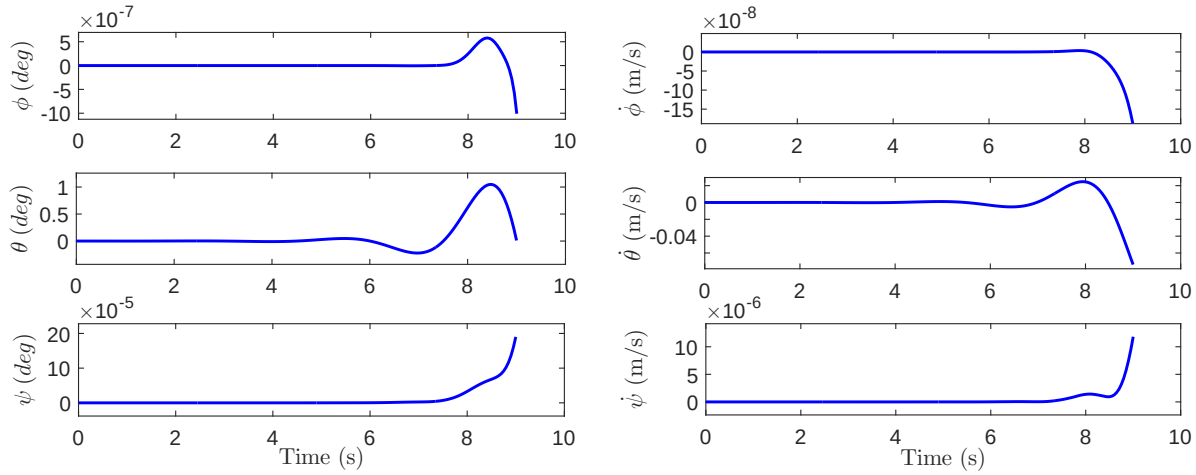

(a) Euler angles with time

(b) Euler angle rates pitch time

Figure 8: Open loop response for symmetric step input to all the rotors (attitude)

B. Experimental Results

In this section, experimental results are provided which substantiates the predictions from the theoretical model developed above

1. Static Experiment

During static experiment, predictions of the thrust and torque from the model developed above are validated by experimentally measuring the thrust and torque of a rotor during hover. Figure 9 shows hover test stand with rotor head mounted on it which is used to measure thrust and torque. The experimental setup consists of a six component load cell mounted on hover test stand with a variable pitch rotor system mounted on top of it. PixHawk microcontroller along with programmable electronic speed controller (ESC) is used to monitor the rotational speed of the rotor during the experiment. Since blade that is used on Assault Reaper 500 is small, the measurement data was affected by ground effect produced due to the load cell which blocks the inflow due to the small rotor mounted above it. Hence validation is done with a larger rectangular rotor (radius = 0.3325 m, chord = 0.32 cm, max t/c=12%) with symmetric airfoil similar to one used on Assault

Reaper 500 VP quadrotor at smaller rotational speeds. The slower speed ensures that the rotor is operating at similar Reynolds number range, with tip Reynolds number of the order of 10^5. Since the airfoil is similar the aerodynamic characteristics of this rotor will also be same as that of the airfoil on Assault Reaper 500.

Figures 10 (a) and 10 (b) show the variation of thrust and torque with blade pitch angle while comparing experimentally measured values with those predicted using BEMT at two different rotational speeds - 1200 RPM and 1500 RPM. It can be observed that the measured thrust and torque values match quite well with the predicted ones.

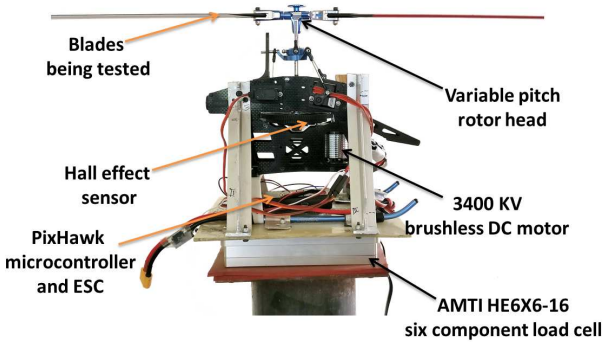

Figure 9: Experimental setup used for thrust and torque measurements

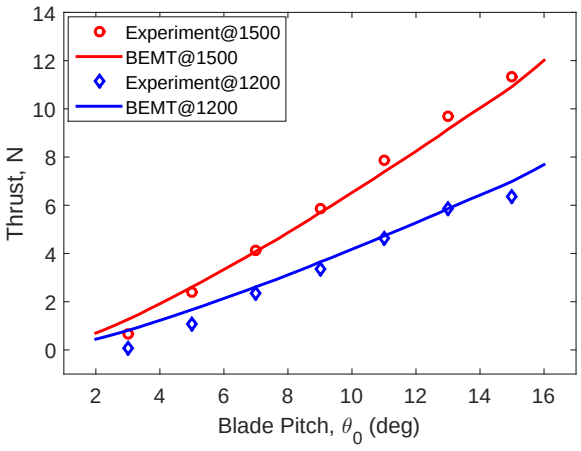

(a) Thrust with blade pitch angle

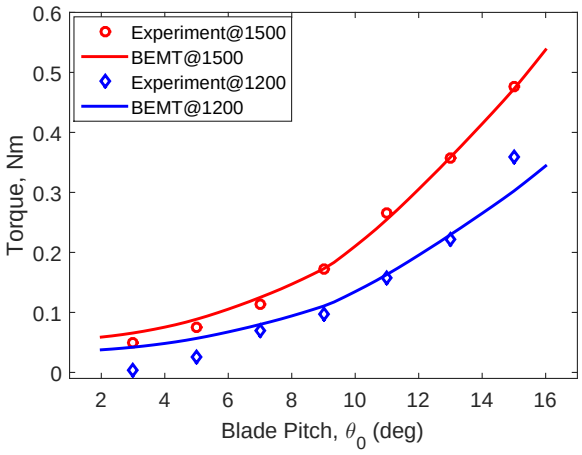

(b) Torque with blade pitch angle

Figure 10: Experimental validation of BEMT

IV. Conclusions

In this paper, development of an advanced flight dynamics model for the variable pitch quadrotor using BEMT and Drees' inflow model is discussed. The open loop response of the quadrotor for a symmetric step input to all the rotors in discussed. The thrust and torque predicted by the aerodynamic model (rotor dynamics) included in the flight dynamic analysis is validated using experimental data collected using a hover test stand. It is found that BEMT based aerodynamic model (rotor dynamics) satisfactorily predicts the thrust and torque for the variable pitch rotor during hover condition. The final paper will include detailed discussion of open loop response of the quadrotor to different set of input combinations at different operating conditions. The final paper will also contain the results of flight experiments for dynamic response of the quadrotor.

References

[1]Albertson, R., Schoenung, S., Fladeland, M., Cutler, F., and Tagg, B., "Enabling earth science measurements with NASA UAS capabilities," *The International Archives of Photogrammetry, Remote Sensing and Spatial Information Sciences*, Vol. 40, No. 7, 2015, pp. 1111.

[2]Schafroth, D., Bouabdallah, S., Bermes, C., and Siegwart, R., "From the test benches to the first prototype of the muFly micro helicopter," *Unmanned Aircraft Systems*, Springer, 2008, pp. 245–260.

[3]Naudin, J.-L., "The GFS UAV Project," `http://jlnlabs.online.fr/gfsuav/index.htm`.

[4]Ozdemir, U., Aktas, Y. O., Demirbag, K., Erdem, A., Kalaycıoglu, G. D., Ozkol, I., and Inalhan, G., "Design of a commercial hybrid VTOL UAV system," *Unmanned Aircraft Systems (ICUAS), 2013 International Conference on*, IEEE, 2013, pp. 214–220.

[5]Stewart, J., "Google Tests Drone Deliveries in Project Wing Trials (August 2014)," `http://www.bbc.com/news/technology-28964260`.

[6]Benedict, M., Jarugumilli, T., and Chopra, I., "Experimental Optimization of MAV-Scale Cycloidal Rotor Performance," *Journal of the American Helicopter Society*, Vol. 56, No. 2, 2011, pp. 22005–22005.

[7]Cutler, M., Ure, N.-K., Michini, B., and How, J., "Comparison of fixed and variable pitch actuators for agile quadrotors," *AIAA Guidance, Navigation, and Control Conference*, 2011, p. 6406.

[8]Pounds, P. and Mahony, R., "Design principles of large quadrotors for practical applications," *Robotics and Automation, 2009. ICRA'09. IEEE International Conference on*, IEEE, 2009, pp. 3265–3270.

[9]Gadekar, R., Duhoon, A., A., A., and Kothari, M., "Design, Development, and Closed-loop Flight-Testing of a Single Power Plant Variable Pitch Quadrotor Unmanned Air Vehicle," *73rd American Helicopter Society Annual Forum*, 2017.

[10]Leishman, J. G., *Principles of Helicopter Aerodynamics*, chap. 2, Cambridge University Press, 2nd ed., 2006, pp. 115–170.

[11]Anonymous, "Quadcopter," `http://en.wikipedia.org/wiki/Quadcopter`.

[12]Michini, B., Redding, J., Ure, N. K., Cutler, M., and How, J. P., "Design and flight testing of an autonomous variable-pitch quadrotor," *Robotics and Automation (ICRA), 2011 IEEE International Conference on*, IEEE, 2011, pp. 2978–2979.

[13]Cutler, M. and How, J., "Actuator constrained trajectory generation and control for variable-pitch quadrotors," *AIAA Guidance, Navigation, and Control Conference*, 2012, p. 4777.

[14]Tao, P., *Design, prototyping and autonomous control of gasoline-engine variable-pitch quadcopter*, Master's thesis, National University of Singapore, Singapore, 2016.

[15]Martinez, V., "Modelling of the flight dynamics of a quadrotor helicopter," *A MSc Thesis in Cranfield University*, Vol. 71, No. 2, 2007, pp. 149–438.

[16]Luo, J., Zhu, L., and Yan, G., "Novel quadrotor forward-flight model based on wake interference," *AIAA Journal*, Vol. 53, No. 12, 2015, pp. 3522–3533.

[17]Gupta, N., Kothari, M., and A., A., "Flight dynamics and nonlinear control design for variable-pitch quadrotors," *American Control Conference (ACC), 2016*, IEEE, 2016, pp. 3150–3155.

[18]Seddon, J. and Newman, S., *Basic Helicopter Aerodynamics*, chap. 5, A John Willey and Sons, Ltd., Publication, 3rd ed., 2011, pp. 111–138.

[19]Ghazirah, B., Razali, R., and Pinang, P., "The Application of Combined Momentum - Blade Element Theory for Aerodynamics Analysis Helicopter Rotor Blade in the Forward Flight," 2006.

[20]Anonymous, "'Airfoil tools' Airfoil Database," `http://m-selig.ae.illinois.edu/ads.html`.